

Optimal control of a MEMS gyroscope based on the Koopman theory

Mehran Rahmani¹ · Sangram Redkar¹

Received: 24 September 2022 / Revised: 27 December 2022 / Accepted: 29 December 2022 © The Author(s), under exclusive licence to Springer-Verlag GmbH Germany, part of Springer Nature 2023

Abstract

Microelectromechanical (MEMS) gyroscopes are small devices used in different industries such as automotive and robotics systems due to their small size and low costs. The MEMS gyroscopes constantly encounter external disturbances, which introduce some mechanical and electromechanical nonlinearity in those systems. In this paper, the Koopman theory is applied to the nonlinear dynamic model of MEMS gyroscope to the linear dynamics model. Dynamic mode decomposition (DMD) is used to obtain eigenfunctions using Koopman's theory to linearize the system. Then, a linear quadratic regulator (LQR) controller is used to control the MEMS gyroscope. The simulation results verify the performance of the proposed controller in terms of high-tracking performance.

Keywords MEMS gyroscope · Dynamic mode decomposition · Nonlinearity · Koopman theory · LQR controller

1 Introduction

A microelectromechanical system (MEMS) gyroscope can effectively perform an important task nowadays, which is detecting and measuring the angular motion of an object. They measure the rate of an object around a particular axis. They have been employed in industrial, automated, and medical applications due to their low cost. The external noises that MEMS gyroscope constantly encounters include temperature change, shock, and vibration. A MEMS gyroscope needs to be developed with an appropriate control technique to suppress the problems [1-3]. Different control systems have been applied to control MEMS gyroscope. Rahmani in [4] proposed a new hybrid fractional sliding mode control to reduce the chattering phenomenon. The main drawback of conventional sliding mode control is creating a chattering phenomenon. A novel parallel control method is applied to reduce the chattering created by the sliding mode controller.

The fractional controller continuously evaluates the error and corrects the error value. Zhou et al. [5] proposed an adap-

tive fuzzy proportional derivative integral (PID) controller to

Mehran Rahmani mrahma61@asu.edu Sangram Redkar sangram.redkar@asu.edu

Published online: 16 January 2023

have the minimum value of the maximum overshoot problem. According to the input error and error change rate, the fuzzy controller online modifies the PID controller's settings. Response time of the gyroscope's closed loop is decreased from 1.09 to 0.54 s, and overshoot is decreased from 20 to 0.004%, with no deterioration of angle random walk or bias instability. Rahmani et al. [6] introduced a compound PID sliding mode control method to control the x and y direction of the MEMS gyroscope. Then, a multi-objective bat algorithm is applied to tune the proposed controller parameters. The proposed control method reduced the chattering phenomenon, improved tracking performance, and reduced maximum overshoot. The mentioned controller methods and most of the other works [7–14] are applied to the linear dynamic model of the MEMS gyroscope.

The Koopman operator is a strong tool for use in complex nonlinear dynamic systems. This theory will use the datadriven method to control nonlinear dynamic systems with high-dimensional nonlinearity [15]. Abraham and Murphey [16] proposed a Koopman-based controller that provides fast learning. They demonstrate the enhanced model-based control performance with an actuated van der Pol system to linearize the nonlinear model by using the Koopman operator. The Koopman operator model of dynamical systems is then used in conjunction with information-theoretic approaches to design a controller for active learning of robot dynamics. It is demonstrated that the active learning controller



The Polytechnic School, Ira Fulton School of Engineering, Arizona State University, Mesa, AZ 85212, USA

accelerates the rate of information concerning the Koopman operator. The proposed method is applied on a real-time quadcopter. Korda and Mezić [17] proposed a novel datadriven method predictor for generating the eigenfunction of the Koopman operator. The predictor thus developed is a linear controlled dynamical system and is easily implementable in the Koopman model predictive control framework to control nonlinear dynamical systems using the linear control method. The numerical simulations verified the controller and predictor performance. Bruder et al. [18] proposed a Koopman-based controller design to control a soft robot. To build explicit dynamical models of soft robotics and control them using model-based control techniques, the Koopman operator theory offers a solution. This method is data-driven, but it produces a control-oriented model that is explicit rather than merely a "black-box" input-output mapping. The control design for soft robotics is discussed in this article along with the Koopman-based system identification methodology used to identify the system. The Koopman-based technique is used to create three controllers for a pneumatic soft robot arm, and their performance is assessed in relation to several practical trajectory-following tasks. These Koopman-based controllers have an average tracking error that is more than three times lower than a benchmark controller built on a linear state-space model of the same system, proving the effectiveness of the Koopman technique in soft robot control. Folkestad and Burdick [19] proposed a nonlinear controller based on Koopman's theory to improve computational efficiency for a planar quadrotor. In [20], the Koopman operator is suggested for the reachability analysis of an autonomous dynamical system. The scholars specifically show how to use the Koopman operator's spectrum analysis, which involves eigenvalues and eigenfunctions, to approximately compute forward and backward accessible sets for an independent dynamical system. The Hausdorff distance between sets, which calculates how far the approximate reachable set is from the actual reachable set, is used to offer formal guarantees for the approximation reachable sets. The Koopman spectrum and the approximate reachable set can be calculated using a computational framework based on convex optimization. The simulation results verified the effectiveness of the proposed method. A common data-driven technique of approximating the Koopman operator's action on a linear function space covered by a dictionary of functions is called extended dynamic mode decomposition (EDMD) [21]. In this study [22], the Koopman operator is used as an emergent pure data-driven modeling strategy to capture the inherent dynamics of the driver-vehicle system and provide an explicit control-oriented driver-vehicle model in an infinitedimensional space. To further increase the finite-dimensional approximation accuracy of the Koopman operator, an online hybrid delay-embedded extended dynamic mode decomposition approach is suggested. Because of the simple linear

structure of the resulting driver—vehicle model, shared controller design is made easier. To gather driving data for the identification and verification of the proposed modeling technique, driver-in-the-loop experiments are carried out on a driving simulator. Experimental findings show the effectiveness and superiority of the suggested modeling approach. Using the Koopman operator on the systems will improve the controller in the data-driven form [23] to have high-tracking performance and less maximum overshoot [24, 25]. The Koopman operator can be used for the linearization of the nonlinear dynamic model.

LQR is an optimal control method that can be used to control the linearized dynamic model [26]. A data-driven paradigm for the linear embedding of nonlinear systems is presented in [27]. The authors provide a systematic, data-driven strategy for developing a linear representation in terms of higher-order derivatives of the underlying nonlinear dynamics by utilizing structural knowledge of generic nonlinear dynamics and the Koopman operator. The nonlinear system is then regulated using an LQR feedback strategy, whose gains only need to be calculated once, using the linear representation. The proposed control method is compared with backstepping control by implementing it on the fish robot. The results verified the proposed control method.

In this paper, an optimal Koopman control method is implemented on a MEMS gyroscope. The main contribution of this paper is to propose a data-driven control method to control a nonlinear MEMS gyroscope, which did not address in any other paper. The contribution of this paper will be described in detail:

- Discussion of nonlinear MEMS gyroscope dynamic models.
- 2 Eigenfunctions obtained by using the DMD method.
- 3 Koopman operator generated by using eigenfunctions obtained from the DMD method.
- 4 A LQR controller used to control created linear dynamics by Koopman theory.
- 5 The performance of the proposed method compares with conventional integral sliding mode control, in which the proposed controller has better performance.

The remaining portions of this work are arranged as follows. Section 2 demonstrates the dynamic model of the MEMS gyroscope. Section 3 presents the sliding mode control method. Section 4 describes the optimal controller based on the Koopman operator. Section 5 shows the simulation results. Section 6 provides the conclusion.

2 Dynamic model of MEMS gyroscope

Figure 1 illustrates a typical z-axis MEMS gyroscope design. The typical MEMS vibratory gyroscope design consists of



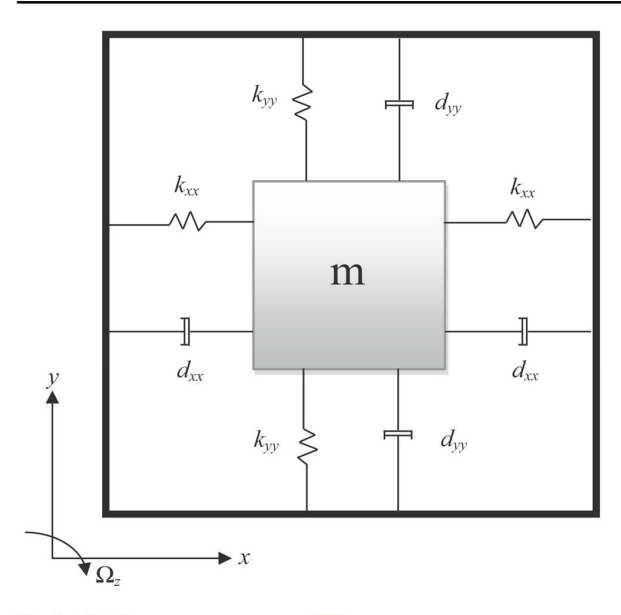


Fig. 1 MEMS gyroscope structure [28]

sensing mechanisms, a proof mass hung by springs, and an electrostatic actuation system for producing an oscillatory motion and measuring the location and velocity of the proof mass [28].

The gyroscope rotates at a slowly varying angular velocity Ω_z , while the proof mass is mounted on a frame that moves with a constant linear velocity. Due to the small displacements x and y, the centrifugal forces $m\Omega_z^2 x$ and $m\Omega_z^2 y$ are predicted to be negligible. The direction in which the Coriolis forces, $2m\Omega_z^*\dot{y}$ and $2m\Omega_z^*\dot{x}$, Are developed is perpendicular to the driving and rotational axes [29, 30]. The following equations determine the dynamics of the gyroscope.

$$m\ddot{x} + d_{xx}^* \dot{x} + d_{xy}^* \dot{y} + k_{xx}^* x + k_{xy}^* y + \beta x^3 = u_x^* + 2m\Omega_z^* \dot{y}$$

$$m\ddot{y} + d_{xy}^* \dot{y} + d_{yy}^* \dot{y} + k_{xy}^* x + k_{yy}^* y + \beta y^3 = u_y^* - 2m\Omega_z^* \dot{x}$$
(2)

Since there is no outside force applied, the origin of the coordinates in Eqs. 1 and 2 is in the center of the proof mass. The asymmetric spring and damping coefficients are represented by the coefficients k_{xy}^* and d_{xy}^* , respectively. The control forces in the x and y direction, u_x^* and u_y^* , are generally known, although they may have small unknown deviations from their nominal values. The spring constants of springs acting in the x and y directions, k_{xx}^* , k_{yy}^* , and damping rates, d_{xx}^* and d_{yy}^* , are also commonly described. Consequently, βx^3 and βy^3 terms will be introduced by both electromechanical and mechanical nonlinearity, in which β is a positive

constant. Equations 1 and 2 could well be represented in vector form as follows:

$$\frac{\ddot{q}^*}{q_0} + \frac{D^*}{m\omega_0}\frac{\dot{q}^*}{q_0} + \frac{K_a}{m\omega_0^2}\frac{q^*}{q_0} + \beta\frac{q^{*3}}{q_0} = \frac{u^*}{m\omega_0^2q_0} - 2\frac{\Omega^*}{\omega_0}\frac{\dot{q}^*}{q_0}$$
(3)

where $q^* = \begin{bmatrix} x^* \\ y^* \end{bmatrix}$, $u = \begin{bmatrix} u_x^* \\ u_y^* \end{bmatrix}$, $\Omega^* = \begin{bmatrix} 0 & -\Omega_z^* \\ \Omega_z^* & 0 \end{bmatrix}$, $D^* = \begin{bmatrix} d_{xx}^* & d_{xy}^* \\ d_{xy}^* & d_{yy}^* \\ d_{xy}^* & d_{yy}^* \end{bmatrix}$, $K_a = \begin{bmatrix} k_{xx}^* & k_{xy}^* \\ k_{xy}^* & k_{yy}^* \end{bmatrix}$, and nondimensional parameters as follows:

$$q = \frac{q^*}{q_0} \quad d_{xy} = \frac{d_{xy}^*}{m\omega_0} \quad \Omega_z = \frac{\Omega_z^*}{\omega_0} \tag{4}$$

$$u_x = \frac{u_x^*}{m\omega_0^2 q_0} \quad u_y = \frac{u_y^*}{m\omega_0^2 q_0} \tag{5}$$

$$\omega_x = \sqrt{\frac{k_{xx}}{m\omega_0^2}} \quad \omega_y = \sqrt{\frac{k_{yy}}{m\omega_0^2}} \quad \omega_{xy} = \frac{k_{xy}}{m\omega_0^2} \tag{6}$$

where the reference length is q_0 and each axis' natural frequency is ω_0 . The MEMS gyroscope's dynamic equations are provided following.

$$\ddot{q} = -(D+2\Omega)\dot{q} - K_b q - \beta q^3 + u + E \tag{7}$$

E is an external perturbation that could be represented as:

$$\ddot{q} = -Y\dot{q} - Pq - \beta q^3 + u + E \tag{8}$$

where $P = K_b$ and $Y = (D + 2\Omega)$ are some parameter variation uncertainties that are determined by ΔY and ΔP . As a result, Eq. (8) could be written as:

$$\ddot{q} = -(Y + \Delta Y)\dot{q} - (P + \Delta P)q - \beta q^3 + u + E \tag{9}$$

where

$$q = \begin{bmatrix} x \\ y \end{bmatrix}, \ u = \begin{bmatrix} u_x \\ u_y \end{bmatrix}, \ \Omega = \begin{bmatrix} 0 & -\Omega_z \\ \Omega_z & 0 \end{bmatrix},$$
$$D = \begin{bmatrix} d_{xx} & d_{xy} \\ d_{xy} & d_{yy} \end{bmatrix}, \ K_b = \begin{bmatrix} \omega_x^2 & \omega_{xy} \\ \omega_{xy} & \omega_y^2 \end{bmatrix}$$

Equation (9) could well be demonstrated as:

$$\ddot{q} = -Y\dot{q} - Pq - \beta q^3 + u(t) + D(t)$$
 (10)

D(t) describes as:

$$D(t) = -\Delta Y \dot{q} - \Delta P q + E \tag{11}$$

3 Integral sliding mode control

A popular and reliable control technique is sliding mode control. Sliding mode control's primary benefits are strong tracking performance and robustness against external perturbations. In most works, sliding mode control has been used with linear dynamic model of MEMS gyroscopes [7, 31]. We apply the sliding mode control on the nonlinear MEMS gyroscope dynamic model. The main part of sliding mode control design is how to select sliding mode surface. The sliding mode surface defines as:

$$\eta = \dot{e} + \lambda \int_{0}^{t} e^{\frac{m}{n}}(\tau) d\tau \tag{12}$$

where e = q, m, n and λ is a positive constant. The equivalent control strategy is obtained when $\dot{\eta} = 0$.

$$\dot{\eta} = \ddot{e} + \lambda e^{\frac{m}{n}} = 0 \tag{13}$$

In Eq. (13), substituting the first and second derivatives from the error will result in the following.

$$\ddot{q} + \lambda q^{\frac{m}{n}} = 0 \tag{14}$$

Equation (10) is substituted with Eq. (14) to generate

$$-Y\dot{q} - Pq - \beta q^{3} + u(t) + D(t) + \lambda q^{\frac{m}{n}} = 0$$
 (15)

The right side of the equation is introduced by moving all elements except u(t).

$$u_{\text{eq}}(t) = Y\dot{q} + Pq + \beta q^3 - D(t) - \lambda q^{\frac{m}{n}}$$
(16)

Equation (16) shows the equivalent controller. Uncertainties in the model and external disruptions cannot be compensated for by the equivalent control. To overcome these problems, a reaching control approach is introduced. The reaching control defines as:

$$u_r(t) = -K_r \eta \tag{17}$$

where K_r is the positive constant.

The control input defines:

$$u(t) = u_{eq}(t) + u_r(t) \tag{18}$$

Sliding mode control is shown to be stable using the Lyapunov theory.

$$L(t) = \frac{1}{2}\eta\eta^{\mathrm{T}} \tag{19}$$

When the controller is stable, the following conditions are met:

$$\dot{L} = \eta^T \dot{\eta} < 0, \, \eta \neq 0 \tag{20}$$

Derivative from Eq. 19 yields

$$\dot{L} = \eta^T \dot{\eta} \tag{21}$$

Substituting Eq. 21 with a derivative of Eq. 19 results in

$$\dot{L} = \eta^T \left(\ddot{e} + \lambda e^{\frac{m}{n}} \right) \tag{22}$$

Equation 22 gave an illustration that

$$\dot{L} = \eta^T \left(\ddot{q} + \lambda q^{\frac{m}{n}} \right) \tag{23}$$

Equation 10 is substituted for Eq. 23 to introduce

$$\dot{L} = \eta^T \left(-Y\dot{q} - Pq - \beta q^3 + u(t) + D(t) + \lambda q^{\frac{m}{n}} \right) \tag{24}$$

Substituting Eq. 18 in Eq. 24produces

$$\dot{L} = \eta^{T} \left(-Y\dot{q} - Pq - \beta q^{3} + u_{\text{eq}}(t) + u_{r}(t) + D(t) + \lambda q^{\frac{m}{n}} \right)$$
(25)

Using Eq. 16 in Eq. 25 shows

$$\dot{L} = \eta^T \left(-Y\dot{q} - Pq - \beta q^3 + Y\dot{q} + Pq + \beta q^3 - D(t) - \lambda q^{\frac{m}{n}} + u_r(t) + D(t) + \lambda q^{\frac{m}{n}} \right)$$
(26)

Simplifying Eq. 26 results in

$$\dot{L} = \eta^T (u_r(t)) \tag{27}$$

Substituting Eq. (17) in Eq. (27) demonstrates

$$\dot{L} = \eta^{T} (-K_{r} \eta) = -K_{r} \eta^{2} \tag{28}$$

Equation (28) shows that $\dot{L} < 0$. Therefore, the condition in Eq. (20) is satisfied and the controller is stable.

4 Optimal control based on the Koopman operator

4.1 Koopman theory

Recently, Koopman operator theory has become a key methodology for deriving data-driven linear representations of nonlinear dynamical systems. For the prediction, estimation, and control of nonlinear systems, it is very encouraging to be able to predict nonlinear dynamics in a linear framework. Numerous traditional findings have been expanded to Koopman formalism [32].

For x and y directions, Eq. (10) could well be expressed as

$$\begin{bmatrix} \ddot{x} \\ \ddot{y} \end{bmatrix} = -\left(\begin{bmatrix} d_{xx} \ d_{xy} \\ d_{xy} \ d_{yy} \end{bmatrix} + \begin{bmatrix} 0 & -2\Omega_z \\ 2\Omega_z & 0 \end{bmatrix} \right) \begin{bmatrix} \dot{x} \\ \dot{y} \end{bmatrix}$$

$$- \begin{bmatrix} \omega_x^2 \ \omega_{xy} \\ \omega_{xy} \ \omega_y^2 \end{bmatrix} \begin{bmatrix} x \\ y \end{bmatrix} - \begin{bmatrix} \beta \ 0 \\ 0 \ \beta \end{bmatrix} \begin{bmatrix} x^3 \\ y^3 \end{bmatrix} \begin{bmatrix} 1 \ 0 \\ 0 \ 1 \end{bmatrix} \begin{bmatrix} u_x \\ u_y \end{bmatrix}$$

$$+ \begin{bmatrix} D(t)_x \\ D(t)_y \end{bmatrix}$$
(29)

The dynamic equations of the first order will be converted from Eq. (27) by choosing the following parameters:

$$\begin{cases} x = z_1 \\ \dot{x} = z_2 \\ y = z_3 \\ \dot{y} = z_4 \end{cases}$$

Then, we have

$$\begin{cases} \dot{z}_{1} = z_{2} \\ \dot{z}_{2} = -\omega_{x}^{2} z_{1} - \beta z_{1}^{3} - d_{xx} z_{2} - \omega_{xy} z_{3} + (2\Omega_{z} - d_{xy}) z_{4} + u_{z_{1}} + D_{z_{1}} \\ \dot{z}_{3} = z_{4} \\ \dot{z}_{4} = -\omega_{xy} z_{1} - (d_{xy} + 2\Omega_{z}) z_{2} - \omega_{y}^{2} z_{3} - \beta z_{3}^{3} - d_{yy} z_{4} + u_{z_{3}} + D_{z_{3}} \end{cases}$$

$$(30)$$

Equation (30) demonstrates

$$\dot{z} = A(z) + Bu \tag{31}$$

The classical form of Eq. (31) can be shown as

$$\frac{\mathrm{d}}{\mathrm{d}t}z(t) = f(z) \tag{32}$$

The dynamics in discrete time are provided by [32]

$$z_{k+1} = F(z_k) \tag{33}$$

where F can be defined as

$$F(z(t_0)) = z(t_0) + \int_{t_0}^{t_0+t} f(z(\tau)) d\tau$$
 (34)

Using the Koopman operator theoretic perspective, the dynamics of a finite-dimensional nonlinear system are lifted to an infinite-dimensional function space, where the development of the original system becomes linear. A component

of an infinite-dimensional Hilbert space known as an observable, g, is a real-valued, scalar measurement function [33]. Based on this observable, the Koopman operator produces

$$Kg = g \circ F \tag{35}$$

A continuous system is available for smooth dynamics.

$$\frac{\mathrm{d}}{\mathrm{d}t}g(z) = Kg(z) = \nabla g(z).f(z) \tag{36}$$

where K is a Koopman operator. The Koopman operator is infinite-dimensional, which is interesting but creates issues for representation and computation. Applied Koopman analysis approximates the evolution on a subspace spanned by a limited number of measurement functions rather than capturing the evolution of all measurement functions in a Hilbert space. By limiting the Koopman operator to an invariant subspace, one may derive a representation of the operator in a finite-dimensional matrix. Any combination of the Koopman operator's eigenfunctions spans a Koopman invariant subspace [32]. When eigenvalue λ is satisfied by the eigenfunction $\varphi(z)$ of the Koopman model.

$$\lambda \varphi(z) = \varphi(F(z)) \tag{37}$$

A Koopman eigenfunction $\varphi(z)$ is satisfied in continuous time.

$$\frac{\mathrm{d}}{\mathrm{d}t}\varphi(z) = \lambda\varphi(z) \tag{38}$$

In existing dynamical systems, obtaining Koopman eigenfunctions from data or analytically is a key issue. The identification of these eigenfunctions makes it easy to characterize nonlinear dynamic systems in terms of these intrinsic observables.

4.2 DMD method

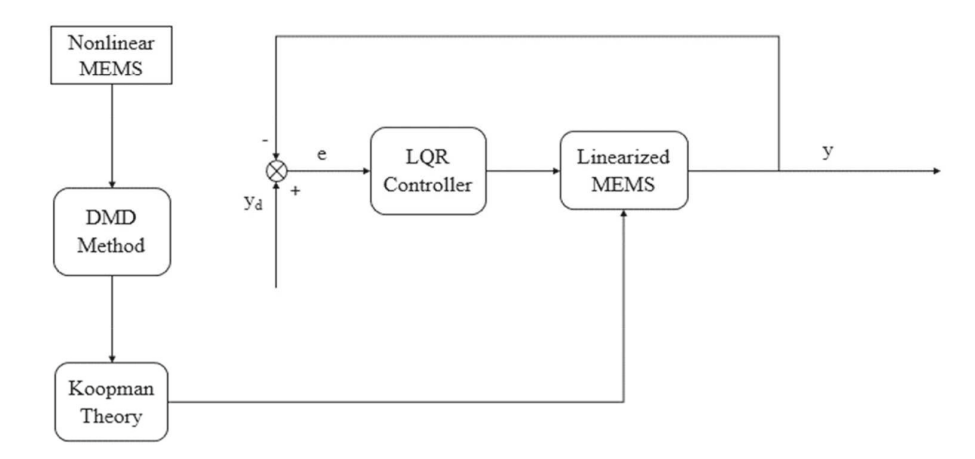
A straightforward numerical approach DMD uses the strongly estimated Koopman operator. The method for estimating the Koopman operator is explained in the following equations:

Equation (31) is solved to get z using Runge–Kutta fourth order. The following equations are then used to construct two spatiotemporal patterns:

$$s_1 = \operatorname{sech}(z+3)\left(e^{2.3ti}\right) \tag{39}$$

$$s_2 = (\operatorname{sech}(z) \tanh(z)) \left(2e^{2.8ti} \right) \tag{40}$$

Fig. 2 Block diagram of the proposed control method



where s defines as:

$$s = s_1 + s_2 \tag{41} \qquad u = -Cy$$

The U_r , S_r , and V_r generate by using a second shortened SVD on s with a truncation rank of 4. The eigenvalues are calculated as:

$$T = U_r' s V_r S_r^{-1} (42)$$

where Φ eigenvalues and Λ eigenvectors will be obtained from . The Koopman operator will be obtained by using the following equation:

$$K = \Phi^{-1} \Lambda \Phi \tag{43}$$

The Koopman operator is generated by Eq. (43). The linear dynamics equation can be defined based on Koopman theory

$$\frac{\mathrm{d}}{\mathrm{d}t}y = Ky + Bu(t) \tag{44}$$

4.3 LQR control

One strategy for making control decisions is LQR, which considers the states of the dynamical system and the control input [34]. The block diagram of the proposed control method is shown in Fig. 2. The goal of the LQR design challenge is to create a state feedback controller that minimizes the objective function. Having a cost function that is

$$J = \int_0^\infty \left(y^T Q y + u^T R u \right) dt \tag{45}$$

where Q and R are the weight matrices [35]. Following is the feedback control law that minimizes the cost function's value:

$$u = -Cy (46)$$

where C defines as:

$$C = R^{-1}B^T P (47)$$

By resolving the continuous time Riccati algebraic equation, P is obtained.

$$K^{T}P + PK + Q - PBR^{-1}B^{T}P = 0 (48)$$

5 Simulation results

Simulation is done using the MATLAB program. The fourthorder Runge–Kutta technique, known as the ode45 order in MATLAB, is used. The integral terminal sliding mode (ITSMC) parameters are chosen as:

$$\lambda = 10, m = 1.25, n = 1.5, \text{ and } K_r = 11.$$

The initial conditions for ITSMC are selected as: $q_{0x} = 0.4$, $q_{0y} = 0.6$, $\dot{q}_{0x} = 0$, and $\dot{q}_{0y} = 0$.

The LQR control items are selected as:

$$A = K, B = \begin{bmatrix} 0 & 1 \\ 1 & 0 \end{bmatrix}, Q = \begin{bmatrix} 1 & 0 \\ 0 & 1 \end{bmatrix}, \text{ and } R = I.$$

The nonlinear model of MEMS gyroscope is controlled by two control methods such as ITSMC and LQR controller linearized by Koopman theory (Koopman-LQR). Figure 3 shows the position tracking of x and y under Koopman-LQR and ITSMC. The Koopman-LQR controller has better performance in comparison with ITSMC in terms of high-tracking performance and low settling time. The Koopman-LQR controller does not have any oscillation in comparison with ITSMC. It demonstrates that the proposed Koopman-LQR has better performance.



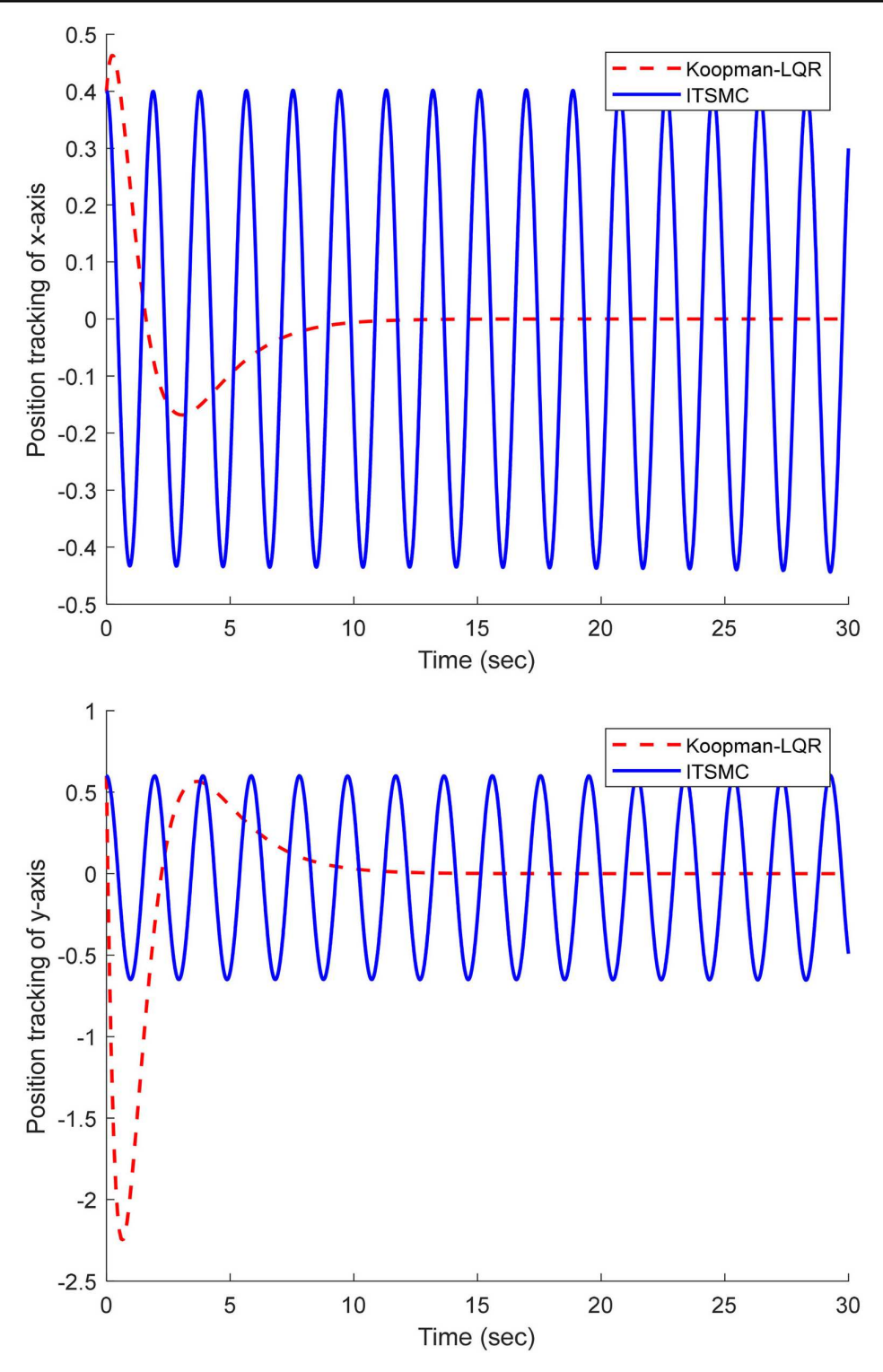


Fig. 3 Position tracking of x- and y-axis under ITSMC and Koopman-LQR controllers



6 Conclusions

This research introduces Koopman-LQR and ITSMC for controlling the nonlinear dynamics of MEMS gyroscopes. First, a nonlinear dynamic model of MEMS gyroscope was introduced. Then, Koopman's theory was used to linearize the nonlinear dynamics of the MEMS gyroscope. The most important part was to calculate the Koopman operator. DMD method was applied to estimate eigenfunction. An LQR controller is used to control the MEMS gyroscope system. The proposed Koopman-LQR method compared with ITSMC had better performance in terms of high tracking, low settling time, and zero oscillation. The effectiveness of the proposed Koopman-LQR method was verified by numerical simulation

Author's contribution All authors contributed to the study conception and design. Material preparation, data collection, and analysis were performed by MR and Dr. SR. The first draft of the manuscript was written by MR and Dr. SR commented on previous versions of the manuscript. All authors read and approved the final manuscript.

Funding This article is based upon work supported by the National Science Foundation (Grant No. 1828010).

Declarations

Conflict of interest There is no conflict of interest.

Ethical Statement I hereby declare that this manuscript is the result of my independent creation under the reviewer's comments. Except for the quoted contents, this manuscript does not contain any research achievements that have been published or written by other individuals or groups. Mehran Rahmani and Sangram Redkar are the only authors of this manuscript. The legal responsibility of this statement shall be borne by me.

References

- Cui J, and Zhao Q (2021) A tactical-grade monolithic horizontal dual-axis mems gyroscope based on off-plane quadrature coupling suppression silicon gratings. In 2021 IEEE 34th International Conference on Micro Electro Mechanical Systems (MEMS) (pp. 814–817). IEEE.
- Wang Z, and Fei J (2021) Double loop neural fractional-order terminal sliding mode control of MEMS Gyroscope. In 2021 Second International Symposium on Instrumentation, Control, Artificial Intelligence, and Robotics (ICA-SYMP) (pp. 1–4). IEEE.
- Varghese PM, and Priya PL (2018) Robust control of a dimensionless dual axis MEMS vibratory gyroscope-a sliding mode approach. In 2018 International CET Conference on Control, Communication, and Computing (IC4) (pp. 57–62). IEEE.
- Rahmani M (2018) MEMS gyroscope control using a novel compound robust control. ISA Trans 72:37–43
- Zhou Y, Fan Q, Liu M, Ren J, Zhou T, Su Y (2021) Design of force-to-rebalanced system with adaptive fuzzy-PID controller for N= 3 MEMS disk gyroscope. IEEE Sens J 21(12):13384–13393

- Rahmani M, Komijani H, Ghanbari A, Ettefagh MM (2018) Optimal novel super-twisting PID sliding mode control of a MEMS gyroscope based on multi-objective bat algorithm. Microsyst Technol 24(6):2835–2846
- Luo S, Yang G, Li J, Ouakad HM (2022) Dynamic analysis, circuit realization and accelerated adaptive backstepping control of the FO MEMS gyroscope. Chaos, Solitons Fractals 155:111735
- Zirkohi MM (2022) Adaptive backstepping control design for MEMS gyroscope based on function approximation techniques with input saturation and output constraints. Comput Electr Eng 97:107547
- Zirkohi MM (2022) Adaptive interval type-2 fuzzy recurrent RBFNN control design using ellipsoidal membership functions with application to MEMS gyroscope. ISA Trans 119:25–40
- Shi Y, Shao X, Zhang W (2020) Neural observer-based quantized output feedback control for MEMS gyroscopes with guaranteed transient performance. Aerosp Sci Technol 105:106055
- Shao X, Shi Y, Zhang W (2021) Input-and-measurement eventtriggered output-feedback chattering reduction control for MEMS gyroscopes. IEEE Trans Syst, Man, Cybern: Syst. 25:54
- Shao X, Shi Y, Zhang W, Cao H (2020) Neurodynamic approximation-based quantized control with improved transient performances for MEMS gyroscopes: theory and experimental results. IEEE Trans Industr Electron 68(10):9972–9983
- Shao X, and Shi Y (2021) Neural-network-based constrained output-feedback control for MEMS gyroscopes considering scarce transmission bandwidth. IEEE Trans Cybern
- Shao X, Si H, Zhang W (2021) Fuzzy wavelet neural control with improved prescribed performance for MEMS gyroscope subject to input quantization. Fuzzy Sets Syst 411:136–154
- Arbabi H (2018) Introduction to Koopman operator theory of dynamical systems. Introduction to Koopman operator theory of dynamical systems.
- Abraham I, Murphey TD (2019) Active learning of dynamics for data-driven control using Koopman operators. IEEE Trans Rob 35(5):1071–1083
- Korda M, Mezić I (2020) Optimal construction of Koopman eigenfunctions for prediction and control. IEEE Trans Autom Control 65(12):5114–5129
- Bruder D, Fu X, Gillespie RB, Remy CD, Vasudevan R (2020)
 Data-driven control of soft robots using koopman operator theory.
 IEEE Trans Rob 37(3):948–961
- Folkestad C, and Burdick JW (2021) Koopman NMPC: Koopmanbased learning and nonlinear model predictive control of controlaffine systems. In 2021 IEEE International Conference on Robotics and Automation (ICRA) (pp. 7350–7356). IEEE.
- Umathe B, Tellez-Castro D, Vaidya U (2022) Reachability analysis using spectrum of Koopman operator. IEEE Control Systems Letters 7:595–600
- Haseli M, Cortés J (2022) Temporal forward-backward consistency, not residual error, measures the prediction accuracy of extended dynamic mode decomposition. IEEE Control Syst Lett 7:649–654
- Guo W, Zhao S, Cao H, Yi B, Song X (2023) Koopman operatorbased driver-vehicle dynamic model for shared control systems. Appl Math Model 114:423–446
- Mamakoukas G, Castano ML, Tan X, Murphey TD (2021) Derivative-based koopman operators for real-time control of robotic systems. IEEE Trans Rob 37(6):2173–2192
- Son SH, Narasingam A, and Kwon JSI (2021) Integration of offset-free control framework with Koopman Lyapunov-based model predictive control. In 2021 American Control Conference (ACC) (pp. 2818–2823). IEEE.
- Goswami D, and Paley DA (2021) Bilinearization, reachability, and optimal control of control-affine nonlinear systems: a Koopman spectral approach. IEEE Trans Autom Control.



- Brunton SL, Brunton BW, Proctor JL, Kutz JN (2016) Koopman invariant subspaces and finite linear representations of nonlinear dynamical systems for control. PLoS One 11(2):e0150171
- Mamakoukas G, Castano M, Tan X, and Murphey T (2019) Local Koopman operators for data-driven control of robotic systems. In Robot: Sci Syst
- Rahmani M, Rahman MH, Nosonovsky M (2020) A new hybrid robust control of MEMS gyroscope. Microsyst Technol 26(3):853–860
- Yan W, Hou S, Fang Y, Fei J (2017) Robust adaptive nonsingular terminal sliding mode control of MEMS gyroscope using fuzzy-neural-network compensator. Int J Mach Learn Cybern 8(4):1287–1299
- Su Y, Xu P, Han G, Si C, Ning J, Yang F (2020) The characteristics and locking process of nonlinear MEMS gyroscopes. Micromachines 11(2):233
- Zhang R, Shao T, Zhao W, Li A, Xu B (2018) Sliding mode control of MEMS gyroscopes using composite learning. Neurocomputing 275:2555–2564
- Kaiser E, Kutz JN, Brunton SL (2021) Data-driven discovery of Koopman eigenfunctions for control. Mach Learn: Sci Technol 2(3):035023
- 33. Snyder G, and Song Z (2021) Koopman operator theory for nonlinear dynamic modeling using dynamic mode decomposition. *arXiv* preprint arXiv:2110.08442.

- Prasad LB, Tyagi B, Gupta HO (2014) Optimal control of nonlinear inverted pendulum system using PID controller and LQR: performance analysis without and with disturbance input. Int J Autom Comput 11(6):661–670
- Anjali BS, Vivek A, Nandagopal JL (2016) Simulation and analysis
 of integral LQR controller for inner control loop design of a fixed
 wing micro aerial vehicle (MAV). Procedia Technol 25:76–83

Springer Nature or its licensor (e.g. a society or other partner) holds exclusive rights to this article under a publishing agreement with the author(s) or other rightsholder(s); author self-archiving of the accepted manuscript version of this article is solely governed by the terms of such publishing agreement and applicable law.

